EPJ D

Recognized by European Physical Society

Atomic, Molecular, Optical and Plasma Physics

Eur. Phys. J. D (2019) 73: 170 DOI: 10.1140/epjd/e2019-90672-4

Resonant excitations of a Bose Einstein condensate in an optical lattice

Citlali Cabrera-Gutiérrez, Eric Michon, Maxime Arnal, Gabriel Chatelain, Vincent Brunaud, Tomasz Kawalec, Juliette Billy, and David Guéry-Odelin

edp sciences

Società Italiana di Fisica

Springer

Eur. Phys. J. D (2019) 73: 170
https://doi.org/10.1140/epjd/e2019-90672-4

THE EUROPEAN PHYSICAL JOURNAL D

Regular Article

Resonant excitations of a Bose Einstein condensate in an optical lattice

Citlali Cabrera-Gutiérrez[1,2], Eric Michon[1,2], Maxime Arnal[1,2], Gabriel Chatelain[1,2], Vincent Brunaud[1,2], Tomasz Kawalec[3], Juliette Billy[1,2], and David Guéry-Odelin[1,2,a]

[1] Université de Toulouse, UPS, Laboratoire Collisions Agrégats Réactivité, IRSAMC, F-31062 Toulouse, France
[2] CNRS, UMR 5589, F-31062 Toulouse, France
[3] Marian Smoluchowski Institute of Physics, Jagiellonian University, Łojasiewicza 11, PL-30348 Kraków, Poland

Received 6 December 2018 / Received in final form 14 June 2019
Published online 16 August 2019

Abstract. We investigate experimentally a Bose Einstein condensate placed in a 1D optical lattice whose phase or amplitude is modulated in a frequency range resonant with the first bands of the band structure. More precisely, we study the effect of the strength of a weak extra external confinement superimposed to the lattice on the 1 and 2-phonon transitions. We identify lines immune or very sensitive to the external confinement despite many orders of magnitude of difference in strength compared to the lattice. We interpret those features and present 1D numerical simulations including atom-atom interactions consistent with the experimental observations. Using the band mapping technique, we also get a direct access to the populations that have undergone n-phonon transitions for each modulation frequency including for non-zero quasi-momentum.

1 Introduction

The physics of cold atoms placed in time-dependent optical lattices enables one to address an incredibly wide variety of phenomena. Many recent cold atom experiments in optical lattices have demonstrated the usefulness of time-dependent modulation to probe or engineer single and many-body states [1–23]. Modulation with frequencies in a range of values different from interband resonances has been used to renormalize the tunneling rate [1–5], to probe the Mott insulator – superfluid transition [6–9], to excite collective modes [10], to drive quantum transport [11,12], to endow a system with new properties including artificial gauge fields [13,14], or to create nontrivial topological band structures [5,15–23] to name a few.

Resonant modulation favors interband transitions [24–28] and band hybridization [29–32]. It has been used as a spectroscopic calibration [25,33,40] and for the manipulation of wave packets [24,26,34,35] using either phase or amplitude modulation. Polychromatic resonant modulation has also been investigated revealing the possible interference between separated excitation paths [36,37]. However, such resonant modulation may cause heating through intra- or interband transitions generated by 2-particle processes [5,38–42]. A detailed understanding of resonant excitations therefore appears essential to exploit the full potentialities of Floquet engineering [5].

For a large amplitude of modulation and a sufficiently deep optical lattice, the classical phase space becomes mixed. This regime has been investigated in the early 2000 to set up experiments dedicated to the observation of dynamical tunneling between stable islands [43–45].

Furthermore, the band structure of a quantum gas in an optical lattice can be modified by atom-atom interactions. When the interaction energy is on the order of the lattice depth, the band structure exhibits a loop structure about the center of the Brillouin zone allowing for dynamical instabilities and possible hysteretic behaviors [46–49].

In this article, we investigate experimentally and numerically resonant interband excitations in a Bose-condensed atomic cloud confined by a 1D modulated optical lattice in the presence of weak interactions. By weak interactions we mean that the interaction energy is much lower than the lattice depth, and that the band structure is not significantly modified by interactions. In addition to the lattice potential, we consider an external weak harmonic confinement. We report here a noticeable sensitivity of the width of the experimental lines of the spectrum to the effect of this extra confinement: the linewidths can strongly vary when the strength of the external confinement varies typically from 10^{-5} to 10^{-7} compared to that of the lattice. We put the emphasis on 1 and 2-phonon transitions and provide detailed studies for the excitations of the first five bands both by phase and amplitude modulation.

The paper is organized as follows. In Section 2, we provide an overview of the relevant features of our

[a] e-mail: david.gueryodelin@gmail.com

experimental setup. The experimental spectra along with their comparison with the numerics are presented in Section 3. In Section 4, we detail our experimental approach and analysis of excitations at non-zero quasi-momentum that may involve multiphonon processes. Two appendices complement the main text, the first one dedicated to the selection rules for interband excitations and the other one to numerical simulations.

2 Overview of the setup

We produce pure rubidium-87 Bose Einstein condensates (BECs) in a hybrid trap, which is the combination of two optical dipole beams and a magnetic trap [50,51]. Along the horizontal optical dipole beam (x-axis), we superimpose the 1D optical lattice which results from the interference of two counter propagating laser beams originating from the same single mode laser (wavelength 1064 nm). All experiments are performed with pure BECs containing typically 10^5 atoms[1]. The excitation is carried out either by phase or amplitude modulation. The lattice potential experienced by the rubidium-87 atoms (of mass m) thus reads

$$V_{\varepsilon,\theta}(x,t) = -V_0(1+\varepsilon(t))\cos^2\left(\frac{\pi x}{d}+\theta(t)\right), \qquad (1)$$

where $d = 532\,\text{nm}$ is the lattice spacing. The lattice potential is made time-dependent through the modulation amplitude $\varepsilon(t)$ and the phase $\theta(t)$. The lattice depth is measured in units of the characteristic energy of the lattice through the dimensionless parameter s_0: $V_0 = s_0\,E_\text{L}$ with $E_\text{L} = h^2/(2md^2)$[2]. The depth of the optical lattice is determined in situ by exciting the intrasite dipole mode as explained in reference [51].

The atoms also experience an external harmonic confinement $m(2\pi\nu_{\text{E}1,2})^2x^2/2$ along the lattice axis, provided by the hybrid trap. Using one or two dipole beams for the hybrid trap, we have the possibility to change the frequency of this extra confinement by slightly more than an order of magnitude. We perform experiments in two different configurations: one with a frequency $\nu_{\text{E}1} = 4\,\text{Hz}$ (single dipole beam configuration) and one with a frequency $\nu_{\text{E}2} = 50\,\text{Hz}$ (crossed dipole beam configuration). There is an extra frequency scale originating from the optical lattice. We evaluate it through the harmonic expansion of the lattice potential about its minima: $\nu_\text{cl} = hs_0^{1/2}/(2md^2) \simeq 14\,\text{kHz}$ for $s_0 = 3$. The ratio of the strength of the external confinement to that of the lattice therefore varies in our experiment from $(\nu_\text{E}/\nu_\text{cl})^2 = 8\times10^{-8}$ to 1.3×10^{-5}.

To engineer the phase and amplitude of the lattice, we use a cascade of Acousto-Optic Modulators. The 15 Watts single mode laser used for the optical lattice is first diffracted by an Acousto-Optic Modulator (AOM_0), and then split into two beams having the same power. Each beam is subsequently diffracted by an AOM before entering into the cell chamber. Those two latter AOMs ($\text{AOMs}_{1,2}$) are driven by two phase-locked synthesizers that imprint their relative phase on the laser light. The modulation amplitude, $\varepsilon(t)$, is realized by tuning the RF power of the AOM_0 while the phase control on $\theta(t)$ is achieved by an appropriate pre-programming of the synthesizers that drive $\text{AOMs}_{1,2}$.

[1] In practice, it means that we can set an upper bound on the temperature on the order of 10 nK.

[2] $E_\text{L} = 4E_\text{R}$ where $E_\text{R} = h^2/(2m\lambda^2)$ with $\lambda = 2d$ is the recoil energy associated to the absorption of a single photon from the laser producing the lattice.

3 Experimental spectra

For a BEC adiabatically loaded into a static optical lattice $V_{0,0}(x)$, the wave function lies in the ground state band. Once the modulation is switched on, interband transitions can occur. Phase and amplitude modulations do not obey the same selection rules for the transfer from a band of index n to n' [25,52] (see Appendix A). For phase modulation ($\theta(t) = \theta_0\sin(\omega t)$), the allowed transitions at the center of the Brillouin zone ($k = 0$) are the following: transition between bands with opposite parity ($n = 1 \to n = 2$, $n = 1 \to n = 4, \ldots$) through 1-phonon transitions, and transition between bands with the same parity through a 2-phonon process. For amplitude modulation ($\varepsilon(t) = \varepsilon_0\sin(\omega t)$), only 1-phonon transitions between bands of identical parity are allowed. We stress that those selection rules are only valid for $k = 0$ and for a potential having a discrete translational symmetry. In Section 4, we provide a direct measurement of the promotion of atoms to excited bands for non-zero quasi-momenta despite a vanishing coupling at $k = 0$ (see Appendix A).

As illustrated in Figure 1, the selection rules can be observed directly on the experimental results. In such an experiment, we load the BEC into an optical lattice of depth s_0 by ramping up progressively the laser intensity in 30 ms [50,51]. The modulation is switched on 2 ms after this adiabatic loading and lasts 1–5 ms for phase modulation and 3–15 ms for amplitude modulation. All confinements are subsequently turned off and an absorption image is taken after a 25 ms time-of-flight. For the modulations, the lattice depth modulation is $\varepsilon_0 = 0.06$ for amplitude modulation and the maximum shift of the position of the lattice is $0.03\,d$ for phase modulation, i.e. $\theta_0 = 0.03\pi$ ($\theta_0 = \pi$ corresponds to a maximum shift of d). The experiment is repeated for many modulation frequencies in the range of interest for a given lattice depth, thus realizing a scan in frequency around the expected interband transitions. The concatenation of those pictures is represented in Figures 1b and 1c for amplitude and phase modulation respectively. Note that all the experiments whose results are shown in Figure 1 have been performed in the presence of an external confinement of frequency $\nu_{\text{E}2} = 50\,\text{Hz}$.

The images taken after the time-of-flight reveal the Fourier space components of the wave function. In the absence of excitation, we simply recover the well-known diffraction pattern of a BEC associated to a periodic structure of lattice spacing d and that exhibits peaks separated by h/d [53]. Even for the deepest lattice depth investigated in this article ($\sim 10\,E_\text{L}$), the diffraction peaks of the interference figure obtained after a long time-of-flight remain

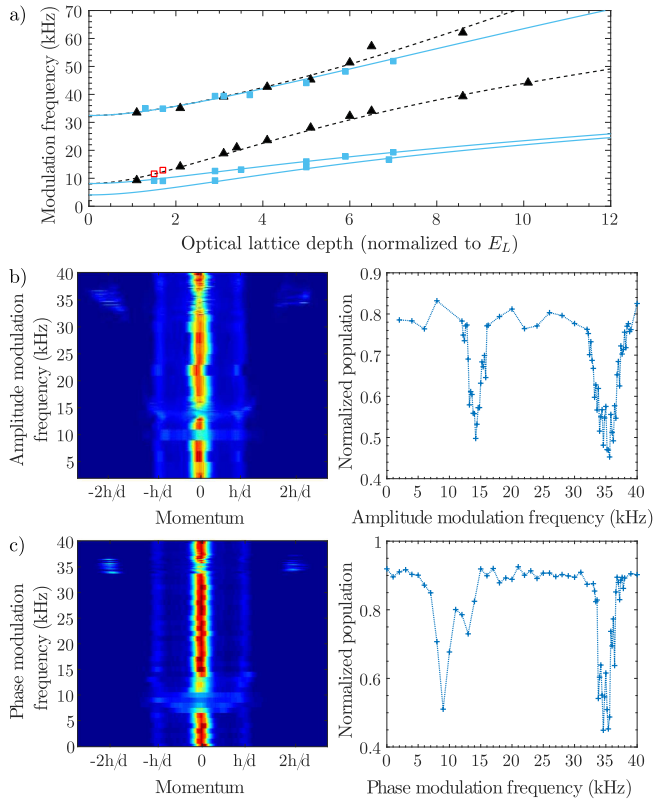

Fig. 1. (a) Summary of the resonances observed experimentally as a function of the lattice depth s_0 (normalized to the lattice characteristic energy E_L) for phase (blue squares) and amplitude (black triangles) modulations. The blue solid (resp. black dashed) line corresponds to the allowed transitions with 1 or 2 phonons for phase (resp. amplitude) modulation. These lines are directly inferred from the band structure of the bare lattice at zero quasi-momentum $k = 0$. The two open red squares correspond to observed excitations through phase modulation, but at frequencies corresponding to an a priori forbidden line for phase modulation. All experiments have been performed in the presence of an external confinement $\nu_{E2} = 50$ Hz. (b) Sample set of experimental data for amplitude modulation ($\varepsilon_0 = 0.06$) for a lattice of normalized depth $s_0 = 2.1$. Left panel: each line of the image corresponds to an experiment performed for a given modulation frequency applied during 15 ms and subsequently imaged after a 25 ms time-of-flight. The experiment is repeated for a modulation frequency ranging from 2 to 40 kHz. Right panel: evolution of the zeroth order diffraction population as a function of the modulation frequency. (c) Similar experimental set of data for phase modulation ($\theta_0 = 0.03\pi$, modulation duration 5 ms) in a lattice of depth $s_0 = 1.7$. The small peak at ∼13 kHz corresponds to an a priori forbidden line; the two other peaks are accounted for with a 1-phonon line.

very well separated [54]. For resonant excitations, atoms acquire a larger energy which results in a depletion of the zeroth order of the diffraction pattern and a concomitant increase of the populations of the higher orders.

To process those images, we extract line by line the population in each diffraction order and infer from the depletion of the zeroth order the resonance frequencies: we determine the center of each zeroth order depletion structure (around 14 and 35 kHz in Fig. 1b for instance) using a Gaussian fit. We find a good agreement between the experimental values and the ones calculated from the band structure spectrum for zero quasi-momentum ($k = 0$) as illustrated in Figure 1a. We also observe directly the selection rules. Indeed, only 1-phonon lines are observed for amplitude modulation while one and two phonon lines can be excited by phase modulation. Note that, at low depth (1.5 and 1.7 E_L), we get an excitation for the phase modulation whose frequency coincides with an a priori forbidden line for phase modulation (see open red squares). This result arises from a first effect of the external confining potential on the excitations: by breaking the translational symmetry, the external confinement weakens the selection rules for phase modulation at low depth.

To investigate in detail the effect of the external confinement, we focus on specific interband transitions. In Figure 2, we have represented two different sets of spectrum data. The lattice depth and amplitude modulation have been chosen to isolate a single line in the considered range of frequencies. Figures 2a and 2b focus on the 1-phonon line from band 1 to 2 for phase modulation ($s_0 = 3.1$, $\theta_0 = 0.03\pi$, duration of the modulation 1 ms, $\nu_{12} = 12.6$ kHz) and Figures 2c and 2d on the second 1-phonon line from band 1 to 5 for amplitude modulation ($s_0 = 3$, $\varepsilon_0 = 0.06$, duration of the modulation 10 ms, $\nu_{15} = 38.9$ kHz). The experimental results are compared to numerical simulations of the 1D Gross-Pitaevskii equation (see Appendix B). The simulations, performed under the same conditions than the experiment, give access to the total energy, plotted as a function of the modulation frequency for the same amplitude of modulation as the one used in experiments. We therefore do not compare strictly speaking the same quantities. However, those two quantities are expected to be closely related.

For phase modulation (Figs. 2a and 2b) the 1-phonon line ($1 \rightarrow 2$, 12.6 kHz) is excited and appears to be essentially immune to the variation of the external confinement equal to $\nu_{E1} = 4$ Hz in Figure 2a and $\nu_{E2} = 50$ Hz in Figure 2b. This result was expected since this line is associated to the excitation of the intrasite dipole mode. Indeed, phase modulation amounts to moving back and forth the position of the sites, it is therefore expected that, for the appropriate frequency, such an excitation drives an oscillatory motion of the center of mass of the wave function inside each site. This interpretation, confirmed by the numerics, provides an explanation for the robustness of this 1-phonon line against both interactions and confinement.

In contrast, the second 1-phonon line for amplitude modulation is spectrally broadened when the external confinement is stronger (compare Figs. 2c and 2d). When the external longitudinal confinement is increased, the wave function tends to localize over a smaller number of sites. The atomic density in each site is consequently increased, and the wave function inside each site departs more and more from the single Bloch state $k = 0$. The condensate therefore spreads over a larger domain of $k \neq 0$ quasi-momentum components [55]. This spreading is directly probed by the resonant modulation and explains the observed increase of the linewidth. In the numerics, the strength of the interactions is accounted for through a

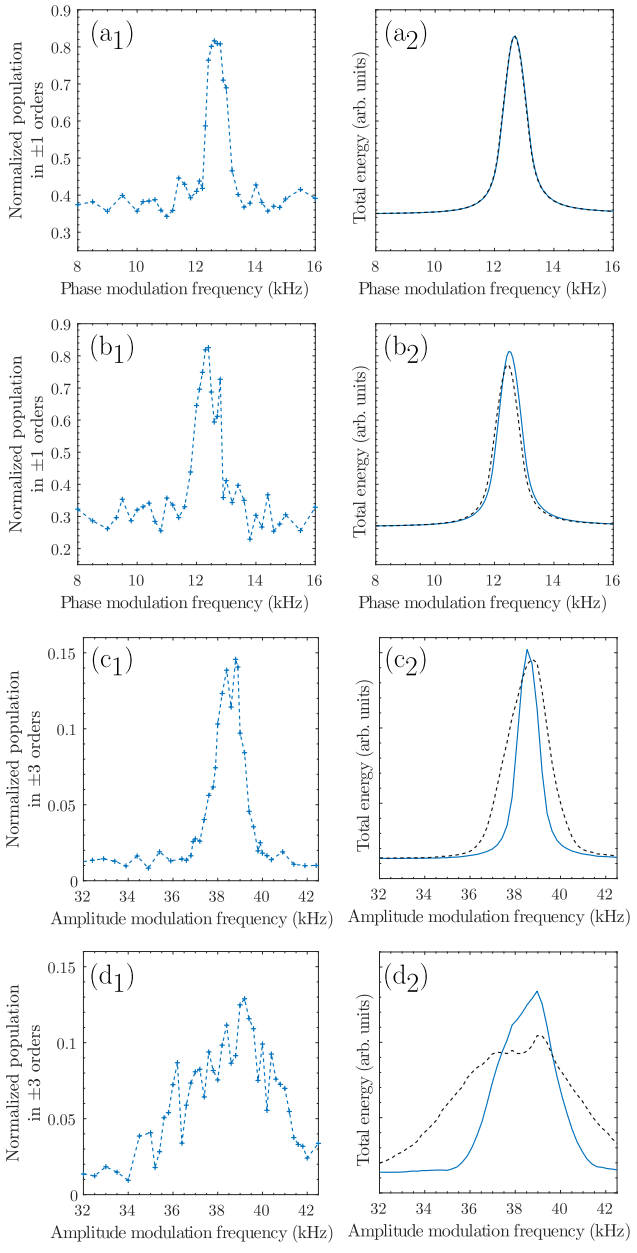

Fig. 2. Spectra. Experimental data corresponding to the normalized populations in high momentum orders (left) and total energy obtained from numerical simulations (right) as a function of the modulation frequency. Simulations performed with a realistic interaction strength ($\beta \simeq 0.4$) are represented by a solid line. Numerical simulations performed in the absence of interactions are represented by the dashed line. (a) and (b) reveal the 1-phonon line from band 1 to 2 obtained for phase modulation; the experimental parameters are $s_0 = 3.1$, $\theta_0 = 0.03\pi$, and the duration of the modulation is 1 ms. (c) and (d) reveal the 1-phonon line from band 1 to 5 observed for amplitude modulation; the experimental parameters are $s_0 = 3$, $\varepsilon_0 = 0.06$, and the duration of the modulation is 10 ms. (a) and (c) ((b) and (d)) correspond to an external confinement of frequency $\nu_{E1} = 4$ Hz ($\nu_{E2} = 50$ Hz).

dimensionless parameter β. For our experimental parameters, $\beta \simeq 0.4$ is chosen to match the size of the condensate measured in the experiment. To distinguish the contribution due to interactions and confinement, we have added in Figure 2 the results of numerical simulations performed on a wave function in the presence (solid line) and in the absence (dashed line) of interactions. By including both interactions and confinement in the numerics, we get numerical results that are consistent with the experimental observations.

4 Non-zero quasi-momentum excitations and multiphonon processes

We now focus on a more detailed excitation spectroscopy, including non-zero quasi-momentum transitions through one and two phonon processes. After such an excitation, the semiclassical local velocity is finite and given by the slope of the energy band:

$$v = v_{\mathrm{L}} \frac{\partial E}{\partial k}, \tag{2}$$

where $v_{\mathrm{L}} = h/md$ is the characteristic velocity associated to the lattice, E is the energy normalized to E_{L} and k the wave vector normalized to $k_{\mathrm{L}}/2 = mv_{\mathrm{L}}/2\hbar$. For instance, the transition from band 1 (ground state) to band 3 (point $A1$ of Fig. 3c) yields a maximum velocity on the order of a few hundreds of $\mu\mathrm{m\,s}^{-1}$. Interestingly, those velocities remain below the sound velocity (estimated to 3 mm/s for our parameters [56,57]) and therefore do not deposit energy into the condensate because of the Landau superfluidity criterium. The size of the condensate being on the order of 150 μm for an external confinement of frequency $\nu_{E2} = 4$ Hz, one shall wait for a very long time, a fraction of a second, to see in position space the excited atoms going out from the condensate. To overcome this limitation, we use the band mapping technique which amounts to accelerate the excited atoms. It consists in decreasing adiabatically the lattice intensity after the modulation [58–60]. As a result, atoms lying on the first band (ground state) have a velocity ranging from 0 to $v_{\mathrm{L}}/2$, those on the second band a velocity ranging from $v_{\mathrm{L}}/2$ to v_{L}, and on the nth band a velocity ranging from $(n-1)v_{\mathrm{L}}/2$ to $nv_{\mathrm{L}}/2$ [26]. With this mapping between velocity and band number, we can identify the different kinds of excitation including the excitation through the absorption of two phonons. As a result of this adiabatic transformation, the atoms promoted by the modulation to higher bands are accelerated and can collide in a dissipative manner with the BEC. However, we do not see heating on the timescale over which the experiment is performed, and thus no evidence for the decay mechanism discussed in references [38–42].

We have carried out such an experiment with an optical lattice of depth $s_0 = 9$ under an amplitude modulation, in the presence of an external confinement of frequency $\nu_{E2} = 4$ Hz. In this experiment, the modulation time is 15 ms and the amplitude of modulation is large: $\varepsilon_0 = 0.23$. As a result, we observe not only the allowed band transition at $k = 0$ but also the ones at $k \neq 0$ that occur

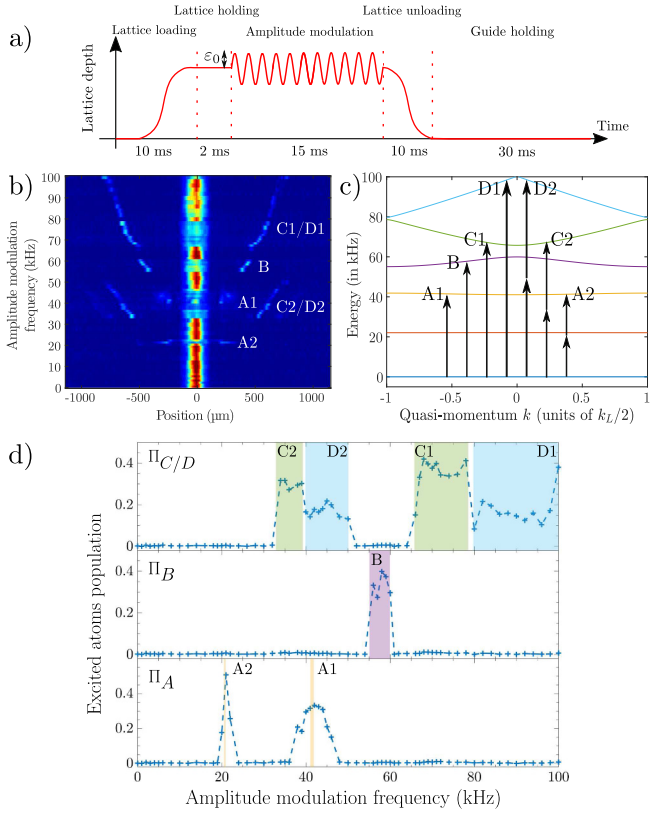

Fig. 3. (a) Sketch of the experimental procedure including the band mapping technique after the amplitude modulation of the optical lattice. (b) In situ experimental images taken after applying the procedure (a) for different values of the frequency of modulation. The amplitude modulation experiment has been here carried out for a lattice of depth $s_0 = 9$ in the presence of an external confinement of frequency $\nu_{E1} = 4\,\mathrm{Hz}$ (c) Band structure associated with this lattice depth. The letters refer to the transitions between the ground state and the excited bands. The number indicates the number of phonons absorbed in the corresponding excitation process. (d) Populations of the excited atoms corresponding to a transfer to bands 3 (A), 4 (B), 5 (C) and 6 (D) as a function of the modulation frequency. The colored areas indicate the 1 and 2-phonon transitions on the whole Brillouin zone.

through 2-phonon transitions. Once the excitation is performed, we decrease the lattice and let the atoms evolve in the presence of the external confinement for 30 ms (see Fig. 3a). This holding time in the guide is smaller than the quarter of period (∼65 ms) associated to the underlying confinement. To directly access the mapping between band number and position, the images are taken without any time-of-flight. Results for each modulation frequency are summarized in Figure 3b.

We have identified the excited bands using letters A, B, C and D followed by a number 1 or 2 denoting the number of phonons involved in the excitation process (see Fig. 3c). For instance, $A1$ corresponds to the 1-phonon transition from band 1 to 3, while $A2$ refers to the 2-phonon transition between the same bands. We indeed observe that $A1$ and $A2$ packets belong to the same range of velocities. The same conclusion holds for $C1$ and $C2$ between bands 1 and 5. The distance over which the packets propagate follows the expected hierarchy: atoms from packet A (band 3) have traveled over a shorter distance than atoms from packet B (band 4), and those of B over a shorter distance than those of packet C (band 5) and D (band 6). This confirms the efficiency of the mapping procedure.

Figure 3d provides the populations Π_A, Π_B and $\Pi_{C/D}$ in the excited bands as a function of the modulation frequency extracted from the image Figure 3b. In practice, the populations Π_i pertain to different velocity classes. To determine them as a function of the modulation frequency, we process each image in the following manner: we extract the maxima of all visible atomic clouds, and integrate the image on areas of width 60 pixels about them. This procedure allows us to take into account the displacement of the atoms due to their velocity. The colored areas indicate the transition frequencies associated to the 1 and 2-phonon lines from the ground state band to the excited bands over the whole Brillouin zone. Interestingly, we recover that the 2-phonon lines (for A, C and D) have a width twice smaller than the 1-phonon line[3]. We get a good understanding of the spectra of Figure 3d based on the 1 and 2-phonon lines. However, the experimental widths for the 1 and 2 phonon A transition turn out to be larger than expected. We attribute this specificity to the large amplitude modulation which tends to enlarge the lines. The method used to extract the populations is not very precise due to non-adiabatic effects near the edges of Brillouin zone, an effect all the more important that the gap is small (for instance between bands 5 and 6). This is a well known limitation of the band mapping technique [61]. It is also delicate to extract the exact velocity with a reasonable accuracy since we do not know exactly at which moment atoms are promoted to the excited band during the 15 ms modulation time.

In conclusion, we have investigated both experimentally and numerically the excitation of atoms in an optical lattice whose phase or amplitude is modulated. We have observed the selection rules and discussed their validity domain. Our study highlights the role of both the confinement and the interactions in the linewidths of the spectra. The band mapping technique has been used to identify non-zero quasi-momentum excitations, and revealed one and two phonon transitions.

This work was supported by Programme Investissements d'Avenir under the program ANR-11-IDEX-0002-02, reference ANR-10-LABX-0037-NEXT, and the research funding grant ANR-17-CE30-0024-01. M.A. acknowledges support from the DGA (Direction Générale de l'Armement).

[3] The width of a given excitation line when it spans a band depends on the number of phonons used to excite it. Indeed, let's assume that with a 1-phonon line we span an interval in frequency ranging for instance from ν_1 to ν_2, so of width $\Delta\nu_{1\mathrm{ph}} = |\nu_2 - \nu_1|$. When we span the same interval with 2 identical phonons each phonon has a frequency that varies from $\nu_1/2$ to $\nu_2/2$. As a result, the width of the corresponding 2-phonon line is $\Delta\nu_{2\mathrm{ph}} = |\nu_2 - \nu_1|/2$.

Author contribution statement

All authors contributed equally to the paper.

Appendix A: Selection rules

The interband transition probability is proportional to the square modulus of the matrix element

$$\delta V_{nn'kk'}(t) = \langle \psi_{n',k'} | \left(V_{\varepsilon,\theta}(x,t) - V_{0,0}(x) \right) | \psi_{n,k} \rangle, \quad \text{(A.1)}$$

where $\{|\psi_{n,k}\rangle\}$ are the Bloch states, n is the band index ($n = 1, 2, \ldots$) and k the quasi-momentum. Bloch states are usually rewritten in terms of the periodic Bloch functions, $u_{n,k}(x)$, as $\psi_{n,k}(x) = e^{ikx} u_{n,k}(x)$ with $u_{n,k}(x+d) = u_{n,k}(x)$. The matrix element (A.1) vanishes as soon as $k \neq k'$, because of the symmetries of the modulation potential and the properties of the Bloch functions.

At the center of the Brillouin zone ($k = 0$), phase and amplitude modulations do not obey the same selection rules for the transfer between bands of index n and n' [25,52].

Consider a phase-modulated optical lattice ($\varepsilon(t) = 0$ and $\theta(t) = \theta_0 \sin(\omega t)$), the lattice potential reads

$$\begin{aligned} V_{0,\theta}(x,t) = & -\frac{V_0}{2} - \frac{V_0}{2}\Bigg\{ \cos\left(\frac{2\pi x}{d}\right) J_0(2\theta_0) \\ & + 2\cos\left(\frac{2\pi x}{d}\right) \sum_{p=1}^{\infty} J_{2p}(2\theta_0) \cos(2p\omega t) \\ & - 2\sin\left(\frac{2\pi x}{d}\right) \sum_{p=0}^{\infty} J_{2p+1}(2\theta_0) \\ & \times \sin((2p+1)\omega t) \Bigg\}, \end{aligned} \quad \text{(A.2)}$$

where $J_p(x)$ is the first kind Bessel function of order p. We first notice that the phase modulation renormalizes the depth of the lattice from V_0 to $V_0 J_0(2\theta_0)$. However, for the amplitude of the phase modulation, θ_0, considered in this article, $J_0(2\theta_0) \simeq 1$, and this renormalization is negligible[4]. As a result, the reasoning for the transition between bands can be performed on the bare lattice (without modulation). In practice, only the first orders play a role since $J_p(x) \sim x^p$ when x is about zero.

For a homogeneous lattice, the Bloch functions $u_{n,0}(x)$ and $u_{n+1,0}(x)$ of two successive bands at $k = 0$ have opposite parities. The last term of equation (A.2) is responsible for a non-zero matrix element between those two successive Bloch functions:

$$\langle u_{n,k=0} | V_{0,\theta}(x,t) | u_{n+1,k=0} \rangle \neq 0. \quad \text{(A.3)}$$

The corresponding interband transition is therefore allowed as a 1-phonon process. Interestingly, the matrix element between bands having the same parity (still at $k = 0$) does not vanish:

$$\langle u_{n,k=0} | V_{0,\theta}(x,t) | u_{n+2,k=0} \rangle \neq 0.$$

[4] The expansion of the zeroth order Bessel function about zero reads $J_0(x) = 1 - x^2/4 + O(x^4)$. For $\theta_0 = 0.03\pi$, we get $J_0(2\theta_0) \simeq 0.9911$.

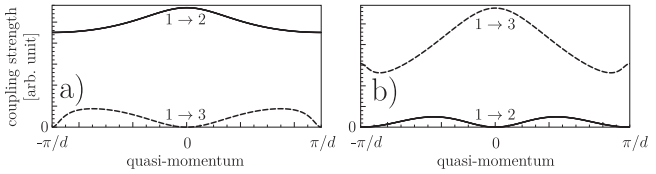

Fig. 4. Coupling strengths $|\delta V_{12kk}|^2$ (solid lines) from band 1 to 2 and $|\delta V_{13kk}|^2$ (dashed lines) from band 1 to 3 for (a) phase modulation and (b) amplitude modulation (lattice depth $s_0 = 3$ in units of E_L (see text and for amplitude modulation, we define the coupling strength between bands n and p as the matrix element $V_{np} = |\langle n,k| \cos^2(\pi x/d) |p,k\rangle|^2$ where $|n,k\rangle$ are the Bloch state, and for phase modulation as $V_{np} = |\langle n,k| \sin(2\pi x/d) |p,k\rangle|^2$ where $|n,k\rangle$).

The first contributing term scales as $\cos(2\omega t)$ revealing the underlying 2-phonon process.

As a result, the phase modulation enables 1-phonon transitions to bands with opposite parity ($n = 1 \to n = 2$, $n = 1 \to n = 4, \ldots$), while the transition to bands with the same parity is allowed through a 2-phonon process.

For amplitude modulation ($\varepsilon(t) = \varepsilon_0 \sin(\omega t)$) the transition strength is given by the matrix element of the modulating term $\varepsilon_0 \cos^2(\pi x/d)$ between the Bloch functions. Only 1-phonon transitions between bands of identical parity are therefore allowed. It is important to note that those selection rules are only valid for $k = 0$ and for a potential having a discrete translational symmetry. In Figure 4, we represent the coupling strengths for phase and amplitude modulation that connects the ground state to the first two excited states as a function of the quasi-momentum k[5]. The 1-phonon selection rules with a vanishing coupling at $k = 0$ are clearly visible: the excitation of the first excited band is prohibited for amplitude modulation but allowed for phase modulation, and vice versa for the second excited band. However, they break down for $k \neq 0$. In practice, when a Bose Einstein condensate is loaded into the lowest band it is not uniquely projected on $k = 0$, but has also components with the same weight on $-k$ and k with $k \neq 0$.

Appendix B: Numerical simulations

The numerical simulations of the 1D time-dependent Gross-Pitaevskii equation are performed using the GPELab Toolbox [62,63]. In practice, we solve the dimensionless equation

$$\begin{aligned} i\frac{\partial \psi}{\partial \tilde{t}} = & \Bigg[\frac{-\Delta + \tilde{\omega}_E^2 X^2}{2} - \tilde{s}(\tilde{t}) \cos^2\left(\frac{\pi X}{4} + \tilde{\theta}(\tilde{t})\right) \\ & + \beta |\psi|^2 \Bigg] \psi \end{aligned} \quad \text{(A.4)}$$

with $X = 4x/d$ the dimensionless position and β a dimensionless parameter which characterizes the strength of the

[5] For amplitude modulation, we define the coupling strength between bands n and p as the matrix element $V_{np} = |\langle n,k| \cos^2(\pi x/d) |p,k\rangle|^2$ where $|n,k\rangle$ are the Bloch state, and for phase modulation as $V_{np} = |\langle n,k| \sin(2\pi x/d) |p,k\rangle|^2$ where $|n,k\rangle$.

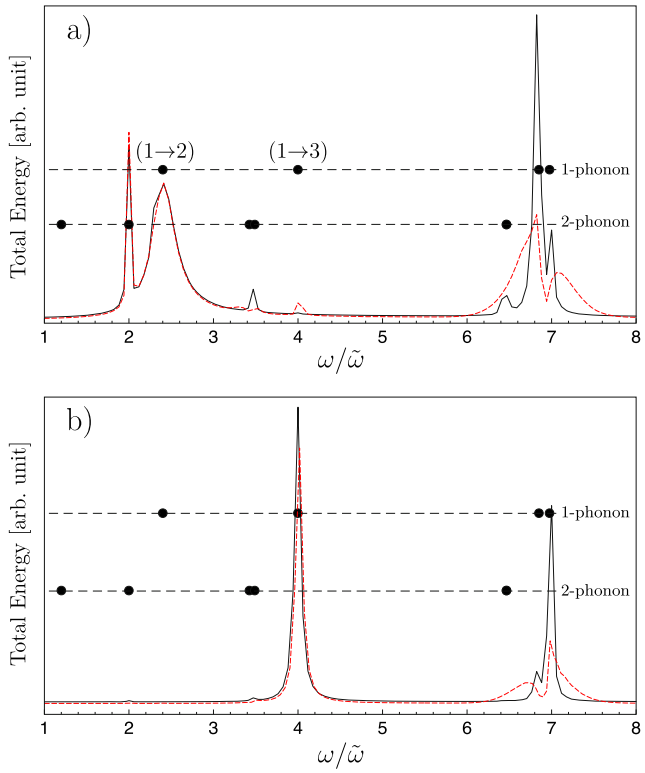

Fig. 5. Numerical results. The total energy associated with the Gross-Pitaevskii equation after the modulation is plotted as a function of the frequency of modulation. The numerics have been performed for an optical lattice of depth $s_0 = 4.86$ for phase (a) and amplitude (b) modulations ($\tilde{\omega} = 2\pi \times 6.55$ kHz, amplitudes of the modulations $\theta_0 = 0.03\pi$ and $\varepsilon_0 = 0.04$), in the presence of an external confinement of frequency $\nu_E = 13.8$ Hz. The solid line corresponds to simulations performed in the presence of repulsive interactions of strength $\beta = 0.8$, and the red dashed line refers to similar simulations but in the absence of interactions ($\beta = 0$). The 1 and 2-phonon transitions inferred from the band structure are represented by black disks.

atomic interactions [50]. The dimensionless time is normalized to $\tilde{t} = \tilde{\omega}t$ with $\tilde{\omega}^{-1} = md^2/(16\hbar) = 24.3\,\mu$s for our parameters, $\tilde{\omega}_E = 2\pi\nu_E/\tilde{\omega}$, and $\tilde{s}_0 = \pi^2 s_0/8$. In practice, we first determine the ground state through an imaginary time evolution for the static lattice potential of depth s_0. We then use this state as an initial condition to run the evolution of the wave function under the time-dependent lattice potential (Eq. (A.4)).

The numerical simulations discussed in this appendix have been carried out for both phase and amplitude modulation with amplitudes of modulation close to that used in experiments ($\varepsilon_0 = 0.04$ and $\theta_0 = 0.03\pi$), in the presence of an external confinement of frequency $\nu_E = 13.8$ Hz. In the main text, we have shown the influence of the confinement on the spectral lines. In the following, we investigate, for a fixed external confinement, the influence of the interaction strength β (see Fig. 5).

For phase modulation (see Fig. 5a), comparing the $\beta = 0$ and $\beta = 0.8$ energy spectra, we find that both the 2-phonon transition at $\omega/\tilde{\omega} \simeq 2$ and the 1-phonon transition at $\omega/\tilde{\omega} \simeq 2.4$ are unaffected by interactions. The interactions modify the other lines. For instance, the 1-phonon transition on the forbidden line at $\omega/\tilde{\omega} \simeq 4$ is washed out, or the 1-phonon transition on the 1–4 line ($\omega/\tilde{\omega} \simeq 6.8$) increases significantly and acquires a reduced width. At first sight, it may appear surprising that interactions yield a narrowing effect on some lines. The reason lies in the homogeneity of the population in each site. Indeed, in the absence of interactions, the BEC occupies only ten sites approximately while with a sufficient amount of repulsive interactions (Thomas Fermi regime), it spreads over a few hundreds of sites. As a result, in the presence of interactions, the BEC is more delocalized and thus closer to a translational invariant system with well defined bands. Excitation lines are consequently much better defined.

As expected from the parity argument, the energy spectrum for amplitude modulation (see Fig. 5b) exhibits lines with opposite selection rules for 1-phonon lines as compared to phase modulation. Similarly to the phase modulation results, we get a transition whose strength is strongly affected by interactions (1-phonon transition from band 1 to 5).

References

1. N. Gemelke, E. Sarajlic, Y. Bidel, S. Hong, S. Chu, Phys. Rev. Lett. **95**, 170404 (2005)
2. H. Lignier, C. Sias, D. Ciampini, Y. Singh, A. Zenesini, O. Morsch, E. Arimondo, Phys. Rev. Lett. **99**, 220403 (2007)
3. E. Kierig, U. Schnorrberger, A. Schietinger, J. Tomkovic, M.K. Oberthaler, Phys. Rev. Lett. **100**, 190405 (2008)
4. E. Michon, C. Cabrera-Gutiérrez, A. Fortun, M. Berger, M. Arnal, V. Brunaud, J. Billy, C. Petitjean, P. Schlagheck, D. Guéry-Odelin, New J. Phys. **20**, 053035 (2018)
5. A. Eckardt, Rev. Mod. Phys. **89**, 011004 (2017)
6. T. Stöferle, H. Moritz, C. Schori, M. Köhl, T. Esslinger, Phys. Rev. Lett. **92**, 130403 (2004)
7. C. Schori, T. Stöferle, H. Moritz, M. Köhl, T. Esslinger, Phys. Rev. Lett. **93**, 240402 (2004)
8. C. Kollath, A. Iucci, T. Giamarchi, W. Hofstetter, U. Schollwöck, Phys. Rev. Lett. **97**, 050402 (2006)
9. N. Fabbri, S.D. Huber, D. Clément, L. Fallani, C. Fort, M. Inguscio, E. Altman, Phys. Rev. Lett. **109**, 055301 (2012)
10. M. Endres, T. Fukuhara, D. Pekker, M. Cheneau, P. Schauβ, C. Gross, E. Demler, S. Kuhr, I. Bloch, Nature **487**, 454 (2012)
11. A. Alberti , V.V. Ivanov, G.M. Tino, G. Ferrari, Nat. Phys. **5**, 547 (2009)
12. E. Haller, R. Hart, M.J. Mark, J.G. Danzl, L. Reichsöllner, H.-C. Nägerl, Phys. Rev. Lett. **104**, 200403 (2010)
13. N. Goldman, J. Dalibard, Phys. Rev. X **4**, 031027 (2014)
14. S. Lellouch, N. Goldman, Quantum Sci. Technol. **3**, 024011 (2018)
15. D.R. Hofstadter, Phys. Rev. B **14**, 2239 (1976)
16. M. Aidelsburger, M. Atala, S. Nascimbène, S. Trotzky, Y.-A. Chen, I. Bloch, Phys. Rev. Lett. **107**, 255301 (2011)
17. M. Aidelsburger, M. Atala, M. Lohse, J.T. Barreiro, B. Paredes, I. Bloch, Phys. Rev. Lett. **111**, 185301 (2013)

18. H. Miyake, G.A. Siviloglou, C.J. Kennedy, W.C. Burton, W. Ketterle, Phys. Rev. Lett. **111**, 185302 (2013)
19. M. Aidelsburger, M. Lohse, C. Schweizer, M. Atala, J.T. Barreiro, S. Nascimbène, N.R. Cooper, I. Bloch, N. Goldman, Nat. Phys. **11**, 162 (2015)
20. F.D.M. Haldane, Phys. Rev. Lett. **61**, 2015 (1988)
21. G. Jotzu, M. Messer, R. Desbuquois, M. Lebrat, T. Uehlinger, D. Greif, T. Esslinger, Nature **515**, 237 (2014)
22. J. Struck, C. Ölschläger, R. Le Targat, P. Soltan-Panahi, A. Eckardt, M. Lewenstein, P. Windpassinger, K. Sengstock, Science **333**, 996 (2011)
23. J. Struck, M. Weinberg, C. Ölschläger, P. Windpassinger, J. Simonet, K. Sengstock, R. Höppner, P. Hauke, A. Eckardt, M. Lewenstein, L. Mathey, Nat. Phys. **9**, 738 (2013)
24. M.C. Fischer, K.W. Madison, Q. Niu, M.G. Raizen, Phys. Rev. A **58**, R2648(R) (1998)
25. M. Weinberg, C. Ölschläger, C. Sträter, S. Prelle, A. Eckardt, K. Sengstock, J. Simonet, Phys. Rev. A **92**, 043621 (2015)
26. P. Cheiney, C.M. Fabre, F. Vermersch, G.L. Gattobigio, R. Mathevet, T. Lahaye, D. Guéry-Odelin, Phys. Rev. A **87**, 013623 (2013)
27. D. Hu, L. Niu, S. Jin, X. Chen, G. Dong, J. Schmiedmayer, X. Zhou, Commun. Phys. **1**, 29 (2018)
28. M. Lacki, J. Zakrzewski, Phys. Rev. Lett. **110**, 065301 (2013)
29. C.V. Parker, L.-C. Ha, C. Chin, Nat. Phys. **9**, 769 (2013)
30. W. Zheng, B. Liu, J. Miao, C. Chin, H. Zhai, Phys. Rev. Lett. **113**, 155303 (2014)
31. L.W. Clark, L. Feng, C. Chin, Science **354**, 606 (2016)
32. B.M. Anderson, L.W. Clark, J. Crawford, A. Glatz, I.S. Aranson, P. Scherpelz, L. Feng, C. Chin, K. Levin, Phys. Rev. Lett. **118**, 220401 (2017)
33. N. Fläschner, M. Tarnowski, B.S. Rem, D. Vogel, K. Sengstock, C. Weitenberg, Phys. Rev. A **97**, 051601 (2018)
34. B.P. Holder, L.E. Reichl, Phys. Rev. A **76**, 013420 (2007)
35. P.L. Pedersen, M. Gajdacz, N. Winter, A.J. Hilliard, J.F. Sherson, J. Arlt, Phys. Rev. A **88**, 023620 (2013)
36. C. Zhuang, C.R. Paul, X. Liu, S. Maneshi, L.S. Cruz, A.M. Steinberg, Phys. Rev. Lett. **111**, 233002 (2013)
37. L. Niu, D. Hu, S. Jin, X. Dong, X. Chen, X. Zhou, Opt. Express **23**, 10064 (2015)
38. S. Choudhury, E.J. Mueller, Phys. Rev. A **90**, 013621 (2014)
39. T. Bilitewski, N.R. Cooper, Phys. Rev. A **91**, 033601 (2015)
40. M. Reitter, J. Näger, K. Wintersperger, C. Sträter, I. Bloch, A. Eckardt, U. Schneider, Phys. Rev. Lett. **119**, 200402 (2017)
41. S. Lellouch, M. Bukov, E. Demler, N. Goldman, Phys. Rev. X **7**, 021015 (2017)
42. T. Boulier, J. Maslek, M. Bukov, C. Bracamontes, E. Magnan, S. Lellouch, E. Demler, N. Goldman, J.V. Porto, Phys. Rev. X **9**, 011047 (2019)
43. D.A. Steck, W.H. Oskay, M.G. Raizen, Science **293**, 274 (2001)
44. W.K. Hensinger, H. Häffner, A. Browaeys, N.R. Heckenberg, K. Helmerson, C. McKenzie, G.J. Milburn, W.D. Phillips, S.L. Rolston, H. Rubinsztein-Dunlop, B. Upcroft, Nature **412**, 52 (2001)
45. R. Dubertrand, J. Billy, D. Guéry-Odelin, B. Georgeot, G. Lemarié, Phys. Rev. A **94**, 043621 (2016)
46. B. Wu, Q. Niu, Phys. Rev. **64**, 061603 (2001)
47. D. Diakonov, L.M. Jensen, C.J. Pethick, H. Smith, Phys. Rev. **66**, 013604 (2002)
48. M. Machholm, C.J. Pethick, H. Smith, Phys. Rev. **67**, 053613 (2003)
49. S.B. Koller, E.A. Goldschmidt, R.C. Brown, R. Wyllie, R.M. Wilson, J.V. Porto, Phys. Rev. A **94**, 063634 (2016)
50. A. Fortun, C. Cabrera-Gutiérrez, G. Condon, E. Michon, J. Billy, D. Guéry-Odelin, Phys. Rev. Lett. **117**, 010401 (2016)
51. C. Cabrera-Gutiérrez, E. Michon, V. Brunaud, T. Kawalec, A. Fortun, M. Arnal, J. Billy, D. Guéry-Odelin, Phys. Rev. A **97**, 043617 (2018)
52. C. Sträter, A. Eckardt, Z. Naturforsch. A **71**, 909 (2016)
53. P. Pedri, L. Pitaevskii, S. Stringari, C. Fort, S. Burger, F.S. Cataliotti, P. Maddaloni, F. Minardi, M. Inguscio, Phys. Rev. Lett. **87**, 220401 (2001)
54. Z. Hadzibabic, S. Stock, B. Battelier, V. Bretin, J. Dalibard, Phys. Rev. Lett. **93**, 180403 (2004)
55. J. Li, Y. Yu, A.M. Dudarev, Q. Niu, New J. Phys. **8**, 154 (2006)
56. B. Wu, Q. Niu, New J. Phys. **5**, 104 (2003)
57. L. Pitaevskii, S. Stringari, B. Einstein, *Condensation and Superfluidity* (Oxford University Press, New York, NY, 2016)
58. M. Greiner, I. Bloch, O. Mandel, T.W. Hänsch, T. Esslinger, Phys. Rev. Lett. **87**, 160405 (2001)
59. J.H. Denschlag, J.E. Simsarian, H. Häffner, C. McKenzie, A. Browaeys, D. Cho, K. Helmerson, S.L. Rolston, W.D. Phillips, J. Phys. B **35**, 3095 (2002)
60. M. Kohl, H. Moritz, T. Stoferle, K. Gunter, T. Esslinger, Phys. Rev. Lett. **94**, 080403 (2005)
61. S.S. Natu, D.C. McKay, B. DeMarco, E.J. Mueller, Phys. Rev. A **85**, 061601 (2012)
62. X. Antoine, R. Duboscq, Comput. Phys. Commun. **185**, 2969 (2014)
63. X. Antoine, R. Duboscq, Comput. Phys. Commun. **193**, 95 (2015)